The impact of detergents on the tissue decellularization process: a ToF-SIMS study

Lisa J White[1,2,#], **Adam J Taylor**[3,4,#], **Denver M Faulk**[2,5], **Tim J Keane**[2,5], **Lindsey T Saldin**[2,5], **Janet E Reing**[2], **Ilea T Swinehart**[2], **Neill J Turner**[2], **Buddy D Ratner**[3,4], and **Stephen F Badylak**[2,5,6]

[1]School of Pharmacy, University of Nottingham, Nottingham, UK

[2]McGowan Institute for Regenerative Medicine, University of Pittsburgh, Pittsburgh, PA

[3]National ESCA and Surface Analysis Center for Biomedical Problems, University of Washington, Seattle, WA

[4]Department of Bioengineering, University of Washington, Seattle, WA

[5]Department of Bioengineering, University of Pittsburgh, Pittsburgh, PA

[6]Department of Surgery, University of Pittsburgh, Pittsburgh, PA

Abstract

Biologic scaffolds are derived from mammalian tissues, which must be decellularized to remove cellular antigens that would otherwise incite an adverse immune response. Although widely used clinically, the optimum balance between cell removal and the disruption of matrix architecture and surface ligand landscape remains a considerable challenge. Here we describe the use of time of flight secondary ion mass spectroscopy (ToF-SIMS) to provide sensitive, molecular specific, localized analysis of detergent decellularized biologic scaffolds. We detected residual detergent fragments, specifically from Triton X-100, sodium deoxycholate and sodium dodecyl sulphate (SDS) in decellularized scaffolds; increased SDS concentrations from 0.1% to 1.0% increased both the intensity of SDS fragments and adverse cell outcomes. We also identified cellular remnants, by detecting phosphate and phosphocholine ions in PAA and CHAPS decellularized scaffolds. The present study demonstrates ToF-SIMS is not only a powerful tool for characterization of biologic scaffold surface molecular functionality, but also enables sensitive assessment of decellularization efficacy.

Keywords

extracellular matrix; biologic scaffold; decellularization; ToF-SIMS; detergents

Correspondence to: Stephen F Badylak.

[#]Authors contributed equally

1. INTRODUCTION

The resident cells of each tissue or organ secrete and maintain an extracellular matrix (ECM) which consists of structural and functional molecules. Interactions between tissue resident cells and the surrounding ECM constitute a state of 'dynamic reciprocity' [1, 2] whereby the ECM provides both structural support and signalling molecules that influence cell behaviour and the local cell populations respond by modifying the ultrastructure and composition of the ECM. Stated differently, the ECM provides tissue-specific molecular and mechanical cues that contribute to the maintenance of cellular homeostasis, promote optimal tissue function and if required, mediate wound healing and tissue repair [3]. Biologic scaffolds composed of ECM are widely used for a variety of clinical applications including breast reconstruction [4, 5], ventral hernia repairs [6, 7], esophageal reconstruction [8, 9], and the replacement of functional skeletal muscle following severe traumatic injury [10, 11], among others [12, 13]. Such biologic scaffolds are prepared by decellularization of tissues and organs to remove cellular antigens capable of inducing an adverse immune response. The objective of any decellularization process is to completely isolate and preserve the extracellular matrix components and structure within a tissue whilst removing all cellular components [14]. In reality, this is an impossible feat as all decellularization methods disrupt ECM ultrastructure and composition through the processes that damage and remove cells and cell debris from tissues. Similarly, complete removal of all cell remnants is not possible and a balance must be achieved between cell removal and the disruption of matrix architecture, and matrix surface ligand landscape.

Preferred methods of decellularization vary amongst tissues and organs due to tissue-specific factors such as tissue size, thickness and shape, and cell and matrix density considerations. One of the most common techniques is immersion in a detergent solution with mechanical agitation to solubilize cell membranes and dissociate DNA and other cellular contents. Detergents have been used to decellularize multiple tissues and organs including tendon [15], esophagus [16, 17], trachea [18, 19], peripheral nerve [20], spinal cord [21, 22], heart valves [23] and dermis [24]. Recently, detergents have been applied in perfusion of whole organs with success in retrograde coronary perfusion in rat [25] and porcine [26] hearts, vascular perfusion in lungs [27] and perfusion via the portal vein in liver [28, 29]. Detergents for decellularization are typically non-ionic, ionic or zwitterionic. Non-ionic detergents, e.g. Triton X-100, disrupt DNA-protein, lipid-lipid and lipid-protein interactions [30] whilst maintaining native protein structures. Ionic detergents, e.g. sodium dodecyl sulfate (SDS) and sodium deoxycholate, completely solubilize cell and nucleic membranes and fully denature proteins [31]. Zwitterionic detergents, e.g. 3-[(3-cholamidopropyl) dimethylammonio]-1-propanesulfonate (CHAPS) have a net zero electrical charge on the hydrophilic head groups which protects the native state of proteins during decellularization and exhibit properties of both ionic and non-ionic detergents [30]. It is logical and expected that use of such detergents will have some disruptive effect upon the ECM during the process of decellularization.

Time of flight secondary ion mass spectrometry (ToF-SIMS) is an analytically sensitive, information-rich surface analytical technique that has been used to investigate various biological samples, from the distribution of proteins and lipids in brain tissue [32] to high

throughput screening of polymer microarrays as cell substrates [33–35]. Recently, ToF-SIMS was utilized to identify differences in cell-secreted matrices [36], to confirm adsorption of complex extracellular matrix coatings [37] and to analyse variances in the surface composition of decellularized tissues from different origins [38, 39]. In ToF-SIMS the surface of interest is bombarded by a primary ion beam (in this study Bi_3^+) which gives rise to characteristic fragments from the top few nanometers of the surface [36]. A proportion of the fragments emitted are charged ions (positive and negative) which may be analysed using a time of flight detector to provide mass/charge spectra characteristic of the surface. Analysis of the spectra provides further information on the chemical moieties, structure and molecular orientation of the surface [40]. During ToF-SIMS analysis, macromolecules on the sample surface are fragmented which often results in spectra containing multiple low mass peaks, rather than individual peaks characteristic of a single component [40]. Translating these low mass peaks into chemical information is challenging.

ToF-SIMS characterization of decellularized ECM scaffolds is particularly challenging due to the chemical and structural complexity of the scaffold surface. Multiple spectra are taken per sample with each spectrum representing a detailed molecular map of the surface. Since the scaffold surface provides the first contact for cells during in vitro culture or upon in-vivo implantation, analysis of the surface molecular chemistry will provide vital insight into the effect of detergent based decellularization. With the availability of ToF-SIMS to probe surface characteristics of materials, the present study aims to (i) use ToF-SIMS to identify differences in the composition of detergent decellularized biologic scaffolds using urinary bladder matrix as a suitable substrate; (ii) correlate these differences with the chemical structure of detergents; (iii) observe residual detergent left behind after the decellularization process and (iv) assess the effect of surface molecular functionality of the detergent decellularized scaffolds upon cell behaviour.

2. METHODS

2.1 Scaffold preparation and decellularization

Porcine urinary bladders were obtained from market weight animals (Tissue Source, Lafayette IN). Bladders were frozen (>24 h at 80°C) and thawed completely before use. To prevent the presence of contaminants in ToF-SIMS analysis, all surfaces, tools and apparatus that came into contact with the bladders were washed in acetone (Fisher) and then methanol (Fisher) prior to use. The basement membrane complex (BMC) and underlying tunica lamina propria of the intact bladder tissue were isolated and harvested as previously described [38, 41, 42]. Briefly, excess connective tissue, adipose tissue and the apex were removed from the bladders using scissors. Bladders were rinsed under running water to remove residual urine and then bisected on one side from the neck to the dome to form a rectangular sheet. The luminal side of the bladder was placed downwards and the tunica serosa, tunica muscularis externa, tunica submucosa and tunica muscularis mucosa were removed by mechanical delamination leaving behind a biologic scaffold composed of intact BMC and tunica lamina propria. The isolated layers were cut into 6 pieces, squares of approximately 5 cm × 5 cm in size for detergent treatment. Samples were subjected to detergent treatments commonly used for decellularization comprising: 3% Triton X-100

(Sigma-Aldrich), 8mM CHAPS (Sigma-Aldrich), 4% sodium deoxycholate (Sigma-Aldrich), 1% sodium dodecyl sulfate (SDS) (Bio-Rad), 0.1% SDS (Bio-Rad) or deionized water for 24 h with physical agitation (orbital shaker at 300 rpm). These selected detergents and concentrations reflect common usage; detergent exposure times have been designed to be less than or equivalent to current experimental practices [15, 18, 19, 21, 31, 43]. An additional group of samples was subjected to 0.1 % peracetic acid (PAA) (Sigma-Aldrich) for 2h and then deionized water for 22 h with physical agitation (300 rpm on an orbital shaker). PAA treatment for 2h has previously been shown to be effective in dissociation of DNA and other cellular components [44]. With the exception of Triton X-100 which was adjusted to a pH of 11.4, all other detergents were utilized at their natural pH. After 24 h treatment, all scaffold groups were subjected to an extensive washing procedure, which was equivalent or exceeded that typically used in decellularization [31]. Scaffolds were rinsed in deionized water for 15 minutes with agitation (300 rpm on orbital shaker). This rinse cycle was repeated three times, to provide a total of 4×15 minute deionized water washes. Each treatment group was then washed for 24 h in deionized water with agitation (300 rpm on orbital shaker). At the end of this wash cycle the 4×15 minute deionized water rinses were repeated and the bladders were then washed for a final 24 hours in deionized water. This extensive washing is equivalent to or exceeds that used commonly in decellularization. The decellularized bladder tissue represents urinary bladder matrix (UBM). The UBM samples were then frozen flat on film, prior to being lyophilized.

2.2 Determination of decellularization efficacy

Lyophilized scaffolds were hydrated prior to fixing in 10% neutral buffered formalin for 24 h. The fixed scaffolds were embedded in paraffin and cut into 5 μm sections onto slides. Slides were stained with hematoxylin and eosin (H&E). Quantification of dsDNA occurred as previously described [45, 46]. Briefly, treated scaffolds were powdered with a Wiley Mill using a 60-mesh. Samples (100 mg) scaffolds were digested in 0.1 mg/ml proteinase K digestion buffer solution for 24 h at 50°C. DNA was extacted twice in phenol/chloroform/isoamyl alcohol and centrifuged at 10,000g for 10 min at 4°C. The top aqueous phase, containing the DNA, was mixed with 3M sodium acetate and 100% ethanol and frozen on dry ice for 20 minutes. Frozen samples were then centrifuged at 4°C for 10 min at 10,000g. The supernatant was poured off and 70% ethanol added. Centrifugation was repeated and the supernatant removed and remaining DNA pellet dried. When dry, the resultant pellet was suspended in TE buffer (10mM Tris/1mM EDTA) and double stranded DNA was quantified in triplicate using Quant-iT PicoGreen Reagent (Invitrogen Corp., Carlsbad, CA, USA) according to the manufacturer's instructions.

2.3 Scanning electron microscopy

Scanning electron microscopy (SEM) was used to examine the surface topology of urinary bladders treated with each detergent. Scaffolds were critical point dried using a Leica EM CPD030 Critical Point Dryer (Leica Microsystems, Buffalo Grove, IL, USA) with carbon dioxide as the transitional medium. Scaffolds were then sputter-coated with a 4.5 nm thick gold/palladium alloy coating using a Sputter Coater 108 Auto (Cressington Scientific Instruments, UK) and imaged with a JEOL JSM6330f scanning electron microscope (JEOL, Peabody, MA, USA).

2.4 Preparation of detergent droplets

ToF-SIMS analysis of detergent samples on inert wafers provided reference detergent spectra for UBM treated scaffolds. Ten cm diameter silicon wafers (Silicon Valley Microelectronics, CA) were scored and diced into 1×1 cm squares. Silicon squares were cleaned by sequential sonication in ultra-pure deionized water, dichloromethane, acetone and methanol, with two x 15 minute washes for each solvent and allowed to dry before use. 200 μl each of 3% Triton X-100, 8 mM CHAPS, 1% SDS, 4% Sodium deoxycholate and stock PAA (15%) was loaded onto the cleaned wafers and allowed to air dry. These detergent loaded wafers were then analysed using the ToF-SIMS conditions described below to provide reference spectra. During ToF-SIMS analysis, the presence of the tissue derived scaffold may alter the ionisation with subsequent fragment peaks observed, including protonated ions of the detergent residues. The characteristic peaks observed on the detergent wafers (reference spectra) were thus utilized in the identification of detergent residues on the UBM samples.

2.5 ToF-SIMS analysis

Each treatment group consisted of individual samples from 5 different bladders. Three representative ~1 cm × 1cm areas were cut from separate UBM samples taken from each treatment group and mounted to the top mount analysis plate using double-sided tape. Positive and negative ion spectra were obtained from the basement membrane side of samples using an ION-TOF V (ION-TOF GmbH) instrument with a 25 keV Bi_3^+ analysis beam mounted at 45° to the sample, with the extractor and flight tube normal to the sample. The primary ion current was 0.8 pA and the total ion dose was kept below 10^{12} ions cm^{-2} to ensure static SIMS conditions. An electron floodgun was used for charge compensation. The area of analysis was 100×100 μm, consisting of 128×128 pixels. Positive and negative spectra were collected over the mass range of m/z 0 – 800. At least three replicates were prepared for each sample type, with at least three spectra obtained from separate sites on each replicate sample. Spectra exhibiting charging issues due to severe topography or very high salt (Na^+) intensities were discarded. At least 10 spectra per treatment condition were retained in each polarity for further analysis. Positive ion spectra were calibrated against peaks for CH_2^+, CH_3^+, $C_3H_2^+$ and $C_4H_3^+$ before further analysis. Negative ion spectra were calibrated against peaks for C^-, C_2^-, C_3^- and C_4^- before further analysis. Supplementary analysis of detergent drops, dried on silicon wafers, was performed in a similar fashion.

2.6 Principal component analysis

Multivariate analysis techniques are mathematical methods that can be used to identify spectral differences and thus improve the specificity and sensitivity of data obtained from complex, multicomponent surfaces [47]. Principal component analysis (PCA) is a multivariate technique that has previously been used to distinguish spectra from lipids in cellular membranes [48], residual ECM proteins following cell lift off [49] and decellularized tissues [38, 39]. In PCA, a set of new variables called principal components (PCs) are calculated which represent new axes in the data space [47, 50] and bisect areas of variance within the original dataset. The largest percentage of variance between groups

within the original dataset will be captured by the first PC. Each subsequent PC is orthogonal to the previous PC and captures sequentially less variance [39].

PCA was performed using the spectragui package of the National ESCA and Surface Analysis Center for Biomedical Problems (NESAC/BIO) MVA Toolbox running in MATLAB R2012a (The MathWorks Inc). Peaks below m/z 500 were manually identified using SurfaceLab 6 (ION-TOF GmbH) and selected in overlaid spectra from each sample set, before adding to a peak list. Peak intensities were compiled into a single-tab separated text file which was then imported into spectragui. Spectra were normalized against the total ion intensity of the peak set and scaled by square-root mean centering before PCA was performed.

2.7 Urothelial cell culture

Lyophilized UBM sheets from each group were cut to 2 cm diameter circles with surgical scissors for use in cell growth studies and were sterilized with ethylene oxide (EtO) gas (16 h cycle at 50 °C in a Series 3plus EOGas Sterilizer, Anderson Sterilizers, Inc., Haw River, NC). Sterilized scaffolds were placed with the BMC luminal surface facing upwards in a 6-well plate. Human urothelial cells (HUCs; purchased from ScienCell, Carlsbad, CA) were cultured in urothelial cell medium (UCM; ScienCell, Carlsbad, CA) containing 1% urothelial growth supplement (ScienCell, Carlsbad, CA) and 1% penicillin/streptomycin solution (ScienCell, Carlsbad, CA). HUCs were cultured in poly-L-lysine coated culture vessels ($2 \mu g/cm^2$) at 37°C and 5% CO_2 and media was changed every other day. After allowing the cells to propagate to sufficient numbers, scaffolds were washed with 1X PBS for 10 minutes twice and then soaked in urothelial cell medium for 4 hours prior to cell seeding. A total of 5×10^5 cells were seeded on the BMC surface of each treatment group in triplicate. Scaffolds were then placed in an incubator at 37°C in 5% CO_2 for 14 days of culture. Culture media was replaced on days 2, 5, 7, 10 and 12. After 7 days and 14 days of culture, cell-seeded scaffolds were fixed in a solution of 4% paraformaldehyde (PFA) in PBS for 30 minutes.

2.8 F-Actin staining and immunolabelling of cell-seeded scaffolds

The fixed 2 cm diameter scaffolds from each treatment group were cut into quarters with surgical scissors and either stained for F-Actin, immunolabelled for E-cadherin or used for apoptosis analysis. Scaffold quarters were washed with 1X PBS prior to permeabilization with 1X PBST (1x PBS with 0.1% Tween and 0.19% Triton) for 10 minutes. Blocking solution (5% goat serum and 1% BSA in PBST) was applied for 30 minutes at room temperature. To visualize the F-actin cytoskeleton, Alexa Fluor® 488 phalloidin (Invitrogen, A12379, 1:40) was added to each scaffold segment for 20 minutes at room temperature. Scaffolds were washed with 1X PBS three times for 5 min each. 4′,6-diamidino-2-phenylindole (DAPI) was used as a nuclear counterstain. Images were taken with a Zeiss Axiovert microscope capturing z-stacks of approximately 20–30 images. An extended focus filter was used to flatten the image and remove out of focus light scattering; images were captured from four random fields across each scaffold.

For E-cadherin immunolabelling the primary antibodies, diluted in blocking solution, were added to scaffold quarters for 16 h at 4°C in a humidified chamber. The slides were then washed three times in PBS prior to the addition of the secondary antibody for 1 h in a humidified chamber at room temperature. DAPI was used as a nuclear counterstain. The primary antibody used was rabbit anti-E-cadherin (Abcam, AB15148. 1:50). The secondary antibody used was Alexa Fluor® goat anti-rabbit 488 (Invitrogen, A11008, 1:400). All primary antibodies were confirmed to cross-react with human epitopes. Scaffold quarters were mounted on coverslips with Prolong® Gold antifade mounting medium (Invitrogen, P36930). Images were taken with a Zeiss Axiovert microscope capturing z-stacks of approximately 20–30 images. An extended focus filter was used to flatten the image and remove out of focus light scattering; images were captured from four random fields across each scaffold.

Determination of apoptosis of HUCs on the BMC was conducted by Click-iT® Plus TUNEL assay for in situ apoptosis detection with Alexa Fluor® dyes (Molecular probes, C10617, C10618, C10619) according to the manufacturer's specifications. Images were taken with a Zeiss Axiovert microscope capturing four random fields across the scaffold.

2.9 Transepithelial electrical resistance measurements

UBM sheets from each group were cut to 8 mm diameter circles, placed into transwell inserts (Corning™ BioCoat™ Assay System, 1.0um membrane) with BMC luminal surface facing upwards and sterilized in situ with ETO gas (16 h cycle at 50 °C in a Series 3plus EOGas Sterilizer, Anderson Sterilizers, Inc., Haw River, NC). For transepithelial electrical resistance measurements Caco-2 cells (passages 24–28, ATCC® HTB-37™) were cultured to approximately 80% confluence in MEM containing non-essential amino acids, 1mM sodium pyruvate, and 20% FBS. Caco-2 cells were seeded on the BMC luminal surface and the functional response was evaluated using a rapid differentiation system (Corning™ Biocoat™ HTS Caco-2 Assay) per manufacturer's instructions. The functional response was measured by transepithelial electrical resistance (TEER). TEER of Caco-2 monolayers was measured with an Epithelial Voltohmmeter (EVOM2, World Precision Instruments). Electrical resistance of each scaffold type without cells was also measured and subtracted from the total electrical resistance determined with the monolayer to calculate the TEER of the monolayer.

2.10 Statistical analysis

ToF-SIMS data shown in PCA scores plots show 95% multivariate confidence intervals. Peak intensity plots show mean (bar), 25th and 75th quartiles (box) with whiskers extending 1.5 interquartile ranges (IQR) beyond them. All other data (apoptosis and TEER) are reported as mean and standard error.

3. RESULTS

3.1 Decellularization efficacy

Imaging of the H&E stained sections showed a reduction in visible nuclei with sodium deoxycholate and 1% SDS treatment (Supplementary Figure 1). Double-stranded DNA

quantification of the scaffolds showed that with the exception of CHAPS, each detergent caused markedly greater removal of the dsDNA compared with treatment by dH_2O or PAA (Supplementary Figure 1A). Scaffolds treated with 1% SDS contained less dsDNA than those treated by any other detergent ($p < 0.05$).

3.2 Detergent treatments produced structural differences in UBM

Scanning electron micrographs showed morphological and structural differences between the UBM scaffolds treated with different detergents. Scaffolds treated with water, 3% Triton X-100 or 4% sodium deoxycholate retained an intricate fibre network (Fig. 1A, C and E) as previously observed [45]. Treatment with PAA and 1% SDS produced an amorphous structure lacking distinct fibres (Fig. 1B and G) whilst treatment with 8 mM CHAPS and 0.1% SDS resulted in a mix of amorphous characteristics with some retained fibre networks.

3.3 Residual detergent fragments are detected by ToF-SIMS

Representative negative ion spectra of UBM scaffolds treated with different detergents are shown in Figure 2. Spectral differences between treatment groups were apparent but also included an intense peak at m/z 79 in native tissue which appeared at low intensities in all treatment groups. Additionally, a notable pair of peaks at m/z 265 and m/z 293 occurred in the spectra of SDS treated UBM; these were not seen in other detergent treatments. Other differences in the spectra were observed but the importance of individual peaks was difficult to assess visually due to the diminishing intensity of peaks at increasing mass.

Principal component analysis (PCA) aids in the identification of peaks characteristic of spectral difference between treatment groups by rotation of the dataset into new variables (principal components) that sequentially describe those with the most variance between treatment groups. Each principal component (PC) is associated with two plots: a scores plot, which describes difference between treatment groups and a loading plot, which describes the contribution of peaks to the PC. The signs of scores and loadings are linked; a sample with negative scores is associated with peaks which have negative loadings.

Scores and loadings plots for the first two principal components of PCA of the negative ion spectra (Fig. 2) are provided in Figure 3. The first principal component (PC1) described 47.6% of the variance in the dataset. UBM scaffolds treated with water, PAA and CHAPS had negative scores which were associated with strongly negatively loading peaks at m/z 63 and 79. These peaks were indicative of phosphate fragments: m/z 63 (PO_2^-) and 79 (PO_3^-). Native (water treated) scaffolds showed the most negative score, followed by PAA and then CHAPS treated samples. All other treatment groups showed positive loadings. PC2 described 25.9% of the variance in the data set. Scaffolds treated with Triton X-100, CHAPS and sodium deoxycholate had negative scores, associated with low mass peaks with strong negative loads including m/z 16, 26 and 42. These peaks were assigned to (O^-), (CN^-) and (CNO^-) respectively. A peak at m/z 391.3 also had a negative loading and this could be assigned as the deprotonated molecular ion of deoxycholate ($C_{24}H_{39}O_4^-$).

Samples treated with both concentrations (0.1 and 1.0 %) of SDS showed positive scores; a larger variance in score occurred with 0.1% SDS treatment. These scores were associated with a range of positively loaded peaks, which included lower mass fragments such as

phosphate fragments at m/z 79 (PO_3^-) and m/z 110 (CH_3PO_4) and sulphate fragments at m/z 80 (SO_3^-), m/z 96 (SO_4^-) and m/z 97 (SO_4 +H)$^-$. Several higher mass peaks also had strong positive loads in PC2. The peak at m/z 265 could be assigned to the SDS molecular ion ($C_{12}H_{25}SO_4^-$), while that at m/z 293 is likely the molecular ion of sodium tetradecyl sulphate ($C_{14}H_{29}SO_4^-$), a common contaminant of SDS [51]. Further principal components of the negative ion spectra did not provide significant separation between treatment groups as can be seen in the scores and loadings plot of PC3, Supplementary Figure 2.

The intensities of residual detergent fragments from sodium deoxycholate, Triton X-100 and SDS are shown in Figure 4; details of the polarity and assignment are provided in Table 1. Analysis of dried detergent spots enabled the identification of the deprotonated deoxycholate molecular ion ($C_{24}H_{39}O_4^-$) at m/z 391.3. This ion was noticeably more intense in the negative ion spectra of UBM treated with deoxycholate (Fig. 4A) compared to any other treatment group. There was considerable variation in the intensity within individual spectra recorded for deoxycholate treated UBM with two outlying points exhibiting three times the mean intensity. These spectra were obtained from the same sample, suggesting that variance within a sample was more significant than spot-to-spot variance on different samples (Fig. 4A).

Analysis of dried detergent spectra (Supplementary Figs. 3 – 5) enabled the identification of the deprotonated molecular ion of Triton X-100 ($C_{14}H_{21}O^-$) at m/z 205.2. There was a greater intensity of this ion in the negative spectra of UBM treated with Triton X-100, compared to other treatment groups (Fig. 4B).

Figures 4C and 4D show the intensity of (SO_4^-) at m/z 79 and ($C_{12}H_{25}SO_4^-$) at m/z 265. These fragments were identified as the sulphate head group of SDS and the SDS molecular ion. Both fragments were uniquely characteristic of SDS in PCA of dried detergent spots (Supplementary Fig. 5) and contributed to the separation of SDS treated UBM samples from other treatment groups in PC2 of PCA of negative ion spectra of UBM (Fig. 3). Intensity of the sulphate head group was low in Triton X-100 and deoxycholate treated UBM. However there appeared to be some intensity of the (SO_4^-) in UBM treated with water, PAA and CHAPS (Fig. 4C). The SDS molecular ion occurred at high intensities in UBM treated with 1% SDS and at much lower intensities in UBM treated with a lower concentration of SDS, 0.1 %.

Representative positive ion spectra of UBM scaffolds treated with different detergents are shown in Supplementary Figure 6. The scores and loadings plots for principal component 1 (PC1) from the positive ion spectra are provided in Figure 5; PC1 described 80.3% of the variance in the dataset and separated water and PAA treated samples, with positive scores, from the other treatment groups, which all scored negatively. Deoxycholate and 1% SDS treated samples showed tighter confidence intervals compared to the other negatively scoring treatment groups: Triton X, CHAPS and 0.1% SDS. Several notable positive loading peaks were associated with phospholipid fragments which included the phospholipid head group ($C_5H_{15}NPO_4^+$) at m/z 184.1 and other associated fragments at m/z 104.1 ($C_5H_{14}NO^+$) and m/z 224.1($C_9H_{19}PO_4^+$). Further principal components of the positive ion spectra did not

provide significant separation between treatment groups as can be seen in the scores and loadings plot of PC2, Supplementary Figure 7.

3.4 Residual nuclear and cell membrane fragments are detected by ToF-SIMS

The intensity of fragments associated with cell membrane and nuclear associated mass peaks are shown in Figure 6; polarity and assignment details are provided in Table 1. Figure 6A shows the intensity of (PO_3^-) at m/z 78.96, a phosphate peak associated with both phospholipids from cell membranes and the phosphate groups in DNA. Figure 6B shows the intensity of a phosphocholine fragment ($C_5H_{15}NPO_4^+$) at m/z 184.12, associated with cell membrane. High intensity of the phosphate and phosphocholine peaks was seen in native (water) and PAA treated UBM and a lower intensity was observed in CHAPS treated UBM. Samples treated with Triton X-100, sodium deoxycholate and 1% SDS show considerably lower intensities, over 90% lower than that observed with water treated UBM.

Both the phosphate and phosphocholine peaks were more intense in samples treated with 0.1% compared to 1% SDS. The phosphate group had a lower intensity in PAA compared to the phosphocholine head group. Other phosphocholine fragments including choline ($C_5H_{14}NO^+$) at m/z 104.1 and glycerophosphocholine ($C_9H_{19}NPO_4^+$) at m/z 224.1 were identifiable in UBM spectra; these fragments showed similar differences in intensity between treatment groups.

3.5 Surface molecular functionality affects cell behaviour

Human urothelial cells (HUC) cultured on the surface of Triton X-100, CHAPS and sodium deoxycholate treated bladders had similar levels of confluence and phenotypic morphology compared to cells cultured on scaffolds treated with deionized water (Fig. 7A). HUC cultured on PAA treated bladders were less confluent with a more rounded morphology (Fig. 7B) compared to deionized water treated scaffolds (Fig. 7A). HUC cultured on bladders treated with SDS had fragmented nuclei and poor morphology and there was reduced cell confluence on SDS treated bladders compared to all other treatment groups (Supplementary Fig. 8A). HUC morphology and confluence worsened with increasing SDS concentrations (Fig. 7F and Fig. 7G) with the highest percentage of apoptotic cells on 1% SDS treated scaffolds (Supplementary Fig. 8A). Additionally, TEER values of Caco-2 cells seeded onto treated bladders showed a lower TEER for SDS treated bladders with increased SDS concentration having a greater effect upon the TEER (Supplementary Fig. 8C).

Although similar levels of confluence and phenotype of HUC were observed with Triton X-100, CHAPS and sodium deoxycholate treated bladders compared to deionized water treatment, tight junction formation of HUC occurred only when HUC were cultured on deionized water treated bladders (Supplementary Fig. 9).

4. DISCUSSION

An acceptable balance must be maintained between using detergents to remove cellular materials and detergent mediated ECM disruption. Ineffective decellularization can induce a strong inflammatory response [44] but excessive damage to ECM ultrastructure, growth factors and critical ECM components can adversely affect cytocompatibility and the ability

to facilitate functional tissue replacement. Non-ionic detergents are effective in cell removal from thin tissues and cause less disruption of ultrastructure and less glycosaminoglycan [52] removal compared to ionic detergents [45, 53]. Ionic detergents are effective in removing nuclear remnants and cytoplasmic proteins from dense tissues but also remove growth factors and GAGs and have been shown to damage collagen and vimentin [54]. Some zwitterionic detergents such as sulfobetaine-10 (SB-10) and sulfobetaine-16 (SB-16) have shown greater ECM preservation and better cell removal than non-ionic detergents [55]; however a recent study showed that the basement membrane integrity of bladders was disrupted similarly by CHAPS or 1% SDS treatment [45].

Although the deleterious effects of detergents upon structure and composition are well-characterized, there is a paucity of information concerning detergent impact upon the functionality of biologic scaffolds. Host remodeling of a biologic scaffold is driven by the initial response of the host cells to the implanted material. The surface topography and ligand landscape of the material will determine the host molecules that are adsorbed to the surface and thus influence subsequent cell behaviour. A comprehensive understanding of the impact of detergents upon surface characteristics is essential for development of successful *in vivo* recellularization strategies and host remodeling of scaffolds and whole organ constructs.

There are currently no regulatory requirements for decellularization which was one of the motivations for the present study. We strongly believe that 'thorough' decellularization is critical for downstream clinical outcomes. Previously we have suggested guidelines for decellularization [30] and published papers on the effects of inadequate decellularization [44]. The study attempts to show the effects of commonly used decellularization agents and bring awareness to the importance of this critical manufacturing step for biologic scaffold materials.

Detergent treatment of UBM samples produced marked changes in fibre network. Only scaffolds treated with Triton X-100 or sodium deoxycholate retained the intricate fibre network present in native UBM samples (Fig. 1). Treatment with CHAPS, SDS and PAA altered collagen fibre organization, with 1% SDS and PAA producing amorphous structures lacking distinct fibres. These changes in the topography of UBM samples added additional complexity to the use of ToF-SIMS to identify compositional differences in detergent decellularized scaffolds. Nonetheless, ToF-SIMS analysis detected residual detergent fragments in UBM scaffolds treated with sodium deoxycholate, SDS and Triton X-100 (Fig. 4). UBM samples treated with either deoxycholate or Triton X-100 showed greater intensity of the respective deprotonated molecular ions compared to other treatments. A sulphate head group, characteristic of SDS treatment was observed in SDS samples. Although there was low intensity in Triton X-100 and sodium deoxycholate samples, some intensity was observed in water, PAA and CHAPS treated bladders but this was likely due to a peak overlap with the phosphate fragment present in these treatment groups. Intensity of the SDS molecular ion clearly separated SDS treated UBM sample from all other treatments; a concentration dependent intensity increase was observed. Evidence of residual CHAPS was not identified in CHAPS treated UBM. Its charge-neutral form may facilitate removal through washing. Additionally CHAPS appeared to be highly susceptible to fragmentation;

low mass fragments under m/z 200 dominated the positive ion spectra (Supplementary Fig. 4) as can be seen in the negative loadings of PC2 (Supplementary Fig. 5A).

In conjunction with ToF-SIMS detection of detergent fragments, this study demonstrated the applicability of ToF-SIMS to detect cell nuclei and cell membrane fragments in biologic scaffolds. ToF-SIMS analysis showed the presence of choline, phosphocholine and glycerophosphocholine ions, which have key roles in the structural integrity of cell membranes in native, PAA and CHAPS treated UBM. Higher intensity of the choline related fragments was observed in water and PAA treated UBM compared to CHAPS (Fig. 6B). Additionally, two phosphate groups, characteristic of cell nuclei, had higher intensities in PAA, CHAPS and water treated UBM, compared to Triton X-100, sodium deoxycholate and SDS treated UBM (Fig. 6A). PAA treated UBM had less intensity of the phosphate group compared to native tissue whereas the intensity of the phosphocholine was similar in both native and PAA treated UBM. This indicates that PAA was more effective in removing cell nuclear material rather than cell membrane components; PAA has previously been shown to be effective in disassociation of DNA from cell nuclei [44]. Since the phosphate and phosphocholine ions are indicative of residual cell debris, the presence of these ions facilitates assessment of decellularization efficacy. Notably, the residual cellular components observed in PAA and CHAPS treated bladders show that these methods of treatment were ineffective at completely removing cellular material from the UBM samples. The most effective removal of cellular material was achieved with 1% SDS and deoxycholate treatment, which was expected given that ionic detergents are effective in removing nuclear remnants [54]. The lower concentration of SDS (0.1%) and non-ionic Triton X-100 had low levels of intensity of the phosphate and phosphocholine ions, indicating that these treatments were not as effective as the higher concentration ionic detergents.

To complement ToF-SIMS analysis, the influence of detergent treatment upon in vitro cell behaviour was also examined. Structurally, the mammalian bladder is a hollow sphere with the innermost layers consisting of the tunica lamina propria and basement membrane lined with the urothelium, a layer of epithelial cells [56]. The urothelium is an example of transitional epithelium and is primarily responsible for providing the permeability barrier in the bladder. Cells are interconnected by tight junctional complexes which restrict paracellular ion support and limit diffusion of proteins [57]. Human urothelial cells in culture acquire a proliferative, regenerative phenotype, which can be manipulated by modification of the culture environment [58]. Previous studies have shown that differentiated urothelial tissues can be generated from normal human urothelial cells propagated in vitro [57, 59, 60]. Culture of human urothelial cells upon UBM scaffolds thus provided an ideal opportunity to assess the *in vitro* response of suitable host cells to the surface topography and ligand landscape of detergent treated urinary bladders. Viability, proliferative capacity and phenotype of HUC were maintained on UBM scaffolds treated with Triton X-100, CHAPS and sodium deoxycholate and was similar to cells cultured on scaffolds treated with deionized water (Fig. 7A). A previous investigation showed that CHAPS and SDS treatment resulted in a basement membrane complex with altered ultrastructure and composition; endothelial cells seeded on CHAPS and SDS treated scaffolds had reduced confluence [45]. In this study, HUC seeded on CHAPS treated bladders maintained confluence and phenotype whereas HUC seeded on bladders treated with PAA were less confluent and had a

more rounded morphology. Peracetic acid is commonly used to disinfect post decellularized tissues but can also act as a decellularizing agent by removing nucleic acids [30]. Recent work utilizing PAA in the generation of tubular small intestinal submucosa (SIS) scaffolds showed that PAA was not effective at decellularization with a 2 hr treatment and that metabolic activity of primary human smooth muscle esophageal cells was much lower on PAA treated SIS compared to untreated SIS [61]; similar conclusions can be drawn from the present study.

HUC cultured on SDS treated bladders had atypical morphology, fragmented nuclei and considerably reduced confluence compared to all other treatment groups. Increasing SDS concentration exacerbated problems with poor cellular morphology and confluence. SDS is an effective decellularization agent and has found application in the decellularization of many tissues and whole organs including tendon [15], lung [62] [63], aorta [64], pulmonary valves [23], kidney [65, 66], liver [67] and recently, retina [68]. However, many studies report deleterious effects of SDS upon ECM ultrastructure [45, 64, 69–72] including reduced collagen, elastin, glycosoaminoglycan (GAG) and growth factor content [45, 67, 73]. Alterations in the structural composition of ECM during decellularization can affect cell attachment, differentiation and function; poor cellular health and reduced functionality have been attributed to matrix alterations caused by SDS decellularization [61, 67, 72]. With the notable exception of Rieder *et al* [74], who showed residual SDS caused massive cell lysis during recellularization, the effect of residual SDS upon cell repopulation has been considered insignificant [23, 72]. Nonetheless, ToF-SIMS detection of SDS fragments in this work indicates that cellular responses may be a result of residual SDS coupled with adverse effects upon the biochemical composition and topographical ligand landscape.

Previous studies have shown that HUC can form stratified cell layers exhibiting tight junctions between cells when cultured in calcium supplemented medium [57] or upon deepithelialized stroma [60]. In this study, HUC maintained viability and phenotype when cultured upon Triton X-100, CHAPS and sodium deoxycholate treated UBM. However, localised intercellular border E-cadherin staining evident of stratification and the formation of tight junctional complexes was only observed when HUC were cultured on deionized water treated bladders. All detergent treatments appeared to affect the ability of HUC to form stratified cell layers in vitro.

5. CONCLUSIONS

ToF-SIMS analysis was used to identify differences in the composition of urinary bladder matrix, a representative biologic scaffold, exposed to detergents; surface molecular functionality was correlated with in vitro cell behaviour. ToF-SIMS analysis, providing high analytical sensitivity molecular specificity and surface localization, showed that Triton X-100, sodium deoxycholate and SDS residual fragments remained after detergent treatment of UBM. It is likely that residual SDS fragments, alongside matrix alterations, contributed to atypical phenotype, lower viability and reduced confluence of human urothelial cells cultured upon SDS treated UBM. Increased SDS concentrations, from 0.1% to 1.0%, increased both the intensity of residual SDS fragments and adverse cell outcomes. ToF-SIMS analysis detected cellular remnants, attributed to nuclear and membrane material, in

PAA and CHAPS treated UBM. Detection of the phosphate and phosphocholine ions facilitates assessment of decellularization efficacy; PAA and CHAPS treatment were ineffective at completely removing cellular material from the UBM samples. This study demonstrates the importance of maintaining a balance between cell removal and detergent disruption of matrix architecture and matrix surface ligand landscape. This study also demonstrates the power of ToF-SIMS for the characterization of decellularized scaffolds and, considering the importance of decellularized bioscaffolds for clinical tissue reconstruction, justifies further studies to achieve the optimum balance between thorough decellularization, maintenance of ECM ultrastructure and biologic functionality.

Supplementary Material

Refer to Web version on PubMed Central for supplementary material.

Acknowledgments

References

1. Bissell MJ, Hall HG, Parry G. How does the extracellular matrix direct gene expression? Journal of theoretical biology. 1982; 99(1):31–68. [PubMed: 6892044]

2. Nelson CM, Bissell MJ. Of Extracellular Matrix, Scaffolds, and Signaling: Tissue Architecture Regulates Development, Homeostasis, and Cancer. Annual Review of Cell and Developmental Biology. 2006; 22(1):287–309.

3. Londono R, Badylak SF. Biologic Scaffolds for Regenerative Medicine: Mechanisms of In vivo Remodeling. Ann Biomed Eng. 2014

4. Israeli R, Feingold RS. Acellular dermal matrix in breast reconstruction in the setting of radiotherapy. Aesthetic surgery journal/the American Society for Aesthetic Plastic surgery. 2011; 31(7 Suppl):51S–64S.

5. Glasberg SB, Light D. AlloDerm and Strattice in breast reconstruction: a comparison and techniques for optimizing outcomes. Plast Reconstr Surg. 2012; 129(6):1223–33. [PubMed: 22327891]

6. Garcia A, Baldoni A. Complex ventral hernia repair with a human acellular dermal matrix and component separation: A case series. Annals of medicine and surgery. 2015; 4(3):271–8. [PubMed: 26288732]

7. Golla D, Russo CC. Outcomes following placement of non-cross-linked porcine-derived acellular dermal matrix in complex ventral hernia repair. International surgery. 2014; 99(3):235–40. [PubMed: 24833145]

8. Nieponice A, Ciotola FF, Nachman F, Jobe BA, Hoppo T, Londono R, Badylak S, Badaloni AE. Patch esophagoplasty: esophageal reconstruction using biologic scaffolds. The Annals of thoracic surgery. 2014; 97(1):283–8. [PubMed: 24266951]

9. Badylak SF, Hoppo T, Nieponice A, Gilbert TW, Davison JM, Jobe BA. Esophageal preservation in five male patients after endoscopic inner-layer circumferential resection in the setting of superficial cancer: a regenerative medicine approach with a biologic scaffold. Tissue Eng Part A. 2011; 17(11–12):1643–50. [PubMed: 21306292]

10. Mase VJ Jr, Hsu JR, Wolf SE, Wenke JC, Baer DG, Owens J, Badylak SF, Walters TJ. Clinical application of an acellular biologic scaffold for surgical repair of a large, traumatic quadriceps femoris muscle defect. Orthopedics. 2010; 33(7):511. [PubMed: 20608620]

11. Sicari BM, Rubin JP, Dearth CL, Wolf MT, Ambrosio F, Boninger M, Turner NJ, Weber DJ, Simpson TW, Wyse A, Brown EH, Dziki JL, Fisher LE, Brown S, Badylak SF. An acellular biologic scaffold promotes skeletal muscle formation in mice and humans with volumetric muscle loss. Science translational medicine. 2014; 6(234):234ra58.

12. Gonfiotti A, Jaus MO, Barale D, Baiguera S, Comin C, Lavorini F, Fontana G, Sibila O, Rombola G, Jungebluth P, Macchiarini P. The first tissue-engineered airway transplantation: 5-year follow-up results. Lancet. 2014; 383(9913):238–44. [PubMed: 24161821]

13. Begum T, Farrelly PJ, Craigie RJ. Non-cross-linked porcine acellular dermal matrix (Strattice Tissue Matrix) in pediatric reconstructive surgery. Journal of pediatric surgery. 2016; 51(3):461–4. [PubMed: 26654170]

14. Gilbert TW. Strategies for tissue and organ decellularization. Journal of Cellular Biochemistry. 2012; 113(7):2217–2222. [PubMed: 22415903]

15. Youngstrom DW, Barrett JG, Jose RR, Kaplan DL. Functional characterization of detergent-decellularized equine tendon extracellular matrix for tissue engineering applications. PLoS One. 2013; 8(5):e64151. [PubMed: 23724028]

16. Keane TJ, Londono R, Carey RM, Carruthers CA, Reing JE, Dearth CL, D'Amore A, Medberry CJ, Badylak SF. Preparation and characterization of a biologic scaffold from esophageal mucosa. Biomaterials. 2013; 34(28):6729–37. [PubMed: 23777917]

17. Keane TJ, DeWard A, Londono R, Saldin LT, Castleton AA, Carey L, Nieponice A, Lagasse E, Badylak SF. Tissue-Specific Effects of Esophageal Extracellular Matrix. Tissue Eng Part A. 2015; 21(17–18):2293–300. [PubMed: 26192009]

18. Baiguera S, Jungebluth P, Burns A, Mavilia C, Haag J, De Coppi P, Macchiarini P. Tissue engineered human tracheas for in vivo implantation. Biomaterials. 2010; 31(34):8931–8. [PubMed: 20800273]

19. Remlinger NT, Czajka CA, Juhas ME, Vorp DA, Stolz DB, Badylak SF, Gilbert S, Gilbert TW. Hydrated xenogeneic decellularized tracheal matrix as a scaffold for tracheal reconstruction. Biomaterials. 2010; 31(13):3520–6. [PubMed: 20144481]

20. Karabekmez FE, Duymaz A, Moran SL. Early clinical outcomes with the use of decellularized nerve allograft for repair of sensory defects within the hand. Hand. 2009; 4(3):245–9. [PubMed: 19412640]

21. Guo SZ, Ren XJ, Wu B, Jiang T. Preparation of the acellular scaffold of the spinal cord and the study of biocompatibility. Spinal cord. 2010; 48(7):576–81. [PubMed: 20065987]

22. Crapo PM, Medberry CJ, Reing JE, Tottey S, van der Merwe Y, Jones KE, Badylak SF. Biologic scaffolds composed of central nervous system extracellular matrix. Biomaterials. 2012; 33(13):3539–3547. [PubMed: 22341938]

23. Cebotari S, Tudorache I, Jaekel T, Hilfiker A, Dorfman S, Ternes W, Haverich A, Lichtenberg A. Detergent decellularization of heart valves for tissue engineering: toxicological effects of residual detergents on human endothelial cells. Artif Organs. 2010; 34(3):206–10. [PubMed: 20447045]

24. Reing JE, Brown BN, Daly KA, Freund JM, Gilbert TW, Hsiong SX, Huber A, Kullas KE, Tottey S, Wolf MT, Badylak SF. The effects of processing methods upon mechanical and biologic properties of porcine dermal extracellular matrix scaffolds. Biomaterials. 2010; 31(33):8626–8633. [PubMed: 20728934]

25. Ott HC, Matthiesen TS, Goh S-K, Black LD, Kren SM, Netoff TI, Taylor DA. Perfusion-decellularized matrix: using nature's platform to engineer a bioartificial heart. Nat Med. 2008; 14(2):213–221. [PubMed: 18193059]

26. Wainwright JM, Hashizume R, Fujimoto KL, Remlinger NT, Pesyna C, Wagner WR, Tobita K, Gilbert TW, Badylak SF. Right ventricular outflow tract repair with a cardiac biologic scaffold. Cells Tissues Organs. 2012; 195(1–2):159–70. [PubMed: 22025093]

27. Ott HC, Clippinger B, Conrad C, Schuetz C, Pomerantseva I, Ikonomou L, Kotton D, Vacanti JP. Regeneration and orthotopic transplantation of a bioartificial lung. Nat Med. 2010; 16(8):927–33. [PubMed: 20628374]

28. Shupe T, Williams M, Brown A, Willenberg B, Petersen BE. Method for the decellularization of intact rat liver. Organogenesis. 2010; 6(2):134–136. [PubMed: 20885860]

29. Uygun BE, Soto-Gutierrez A, Yagi H, Izamis M-L, Guzzardi MA, Shulman C, Milwid J, Kobayashi N, Tilles A, Berthiaume F, Hertl M, Nahmias Y, Yarmush ML, Uygun K. Organ reengineering through development of a transplantable recellularized liver graft using decellularized liver matrix. Nat Med. 2010; 16(7):814–820. [PubMed: 20543851]

30. Crapo PM, Gilbert TW, Badylak SF. An overview of tissue and whole organ decellularization processes. Biomaterials. 2011; 32(12):3233–3243. [PubMed: 21296410]

31. Keane TJ, Swinehart IT, Badylak SF. Methods of tissue decellularization used for preparation of biologic scaffolds and in vivo relevance. Methods. 2015

32. Carlred L, Gunnarsson A, Sole-Domenech S, Johansson B, Vukojevic V, Terenius L, Codita A, Winblad B, Schalling M, Hook F, Sjovall P. Simultaneous imaging of amyloid-beta and lipids in brain tissue using antibody-coupled liposomes and time-of-flight secondary ion mass spectrometry. J Am Chem Soc. 2014; 136(28):9973–81. [PubMed: 24941267]

33. Celiz AD, Smith JG, Patel AK, Hook AL, Rajamohan D, George VT, Flatt L, Patel MJ, Epa VC, Singh T, Langer R, Anderson DG, Allen ND, Hay DC, Winkler DA, Barrett DA, Davies MC, Young LE, Denning C, Alexander MR. Discovery of a Novel Polymer for Human Pluripotent Stem Cell Expansion and Multilineage Differentiation. Adv Mater. 2015; 27(27):4006–12. [PubMed: 26033422]

34. Patel AK, Celiz AD, Rajamohan D, Anderson DG, Langer R, Davies MC, Alexander MR, Denning C. A defined synthetic substrate for serum-free culture of human stem cell derived cardiomyocytes with improved functional maturity identified using combinatorial materials microarrays. Biomaterials. 2015; 61:257–65. [PubMed: 26005764]

35. Hook AL, Williams PM, Alexander MR, Scurr DJ. Multivariate ToF-SIMS image analysis of polymer microarrays and protein adsorption. Biointerphases. 2015; 10(1):019005. [PubMed: 25708635]

36. Taylor AJ, Ratner BD, Buttery LD, Alexander MR. Revealing cytokine-induced changes in the extracellular matrix with secondary ion mass spectrometry. Acta Biomater. 2015; 14:70–83. [PubMed: 25523877]

37. DeQuach JA, Mezzano V, Miglani A, Lange S, Keller GM, Sheikh F, Christman KL. Simple and high yielding method for preparing tissue specific extracellular matrix coatings for cell culture. PLoS One. 2010; 5(9):e13039. [PubMed: 20885963]

38. Brown BN, Barnes CA, Kasick RT, Michel R, Gilbert TW, Beer-Stolz D, Castner DG, Ratner BD, Badylak SF. Surface characterization of extracellular matrix scaffolds. Biomaterials. 2010; 31(3):428–37. [PubMed: 19828192]

39. Barnes CA, Brison J, Michel R, Brown BN, Castner DG, Badylak SF, Ratner BD. The surface molecular functionality of decellularized extracellular matrices. Biomaterials. 2011; 32(1):137–143. [PubMed: 21055805]

40. Ilin Y, Kraft ML. Secondary ion mass spectrometry and Raman spectroscopy for tissue engineering applications. Curr Opin Biotechnol. 2015; 31:108–16. [PubMed: 25462628]

41. Freytes DO, Tullius RS, Badylak SF. Effect of storage upon material properties of lyophilized porcine extracellular matrix derived from the urinary bladder. J Biomed Mater Res B Appl Biomater. 2006; 78(2):327–33. [PubMed: 16365866]

42. Brown B, Lindberg K, Reing J, Stolz DB, Badylak SF. The basement membrane component of biologic scaffolds derived from extracellular matrix. Tissue Eng. 2006; 12(3):519–26. [PubMed: 16579685]

43. Petersen TH, Calle EA, Zhao L, Lee EJ, Gui L, Raredon MB, Gavrilov K, Yi T, Zhuang ZW, Breuer C, Herzog E, Niklason LE. Tissue-Engineered Lungs for in Vivo Implantation. Science. 2010; 329(5991):538–541. [PubMed: 20576850]

44. Keane TJ, Londono R, Turner NJ, Badylak SF. Consequences of ineffective decellularization of biologic scaffolds on the host response. Biomaterials. 2012; 33(6):1771–1781. [PubMed: 22137126]

45. Faulk DM, Carruthers CA, Warner HJ, Kramer CR, Reing JE, Zhang L, D'Amore A, Badylak SF. The effect of detergents on the basement membrane complex of a biologic scaffold material. Acta Biomater. 2014; 10(1):183–93. [PubMed: 24055455]

46. Keane TJ, Dziki J, Castelton A, Faulk DM, Messerschmidt V, Londono R, Reing JE, Velankar SS, Badylak SF. Preparation and characterization of a biologic scaffold and hydrogel derived from colonic mucosa. J Biomed Mater Res B Appl Biomater. 2015

47. Graham DJ, Castner DG. Multivariate analysis of ToF-SIMS data from multicomponent systems: the why, when, and how. Biointerphases. 2012; 7(1–4):49. [PubMed: 22893234]

48. Anderton CR, Vaezian B, Lou K, Frisz JF, Kraft ML. Identification of a lipid-related peak set to enhance the interpretation of TOF-SIMS data from model and cellular membranes. Surface and Interface Analysis. 2012; 44(3):322–333.

49. Canavan HE, Graham DJ, Cheng X, Ratner BD, Castner DG. Comparison of native extracellular matrix with adsorbed protein films using secondary ion mass spectrometry. Langmuir: the ACS journal of surfaces and colloids. 2007; 23(1):50–6. [PubMed: 17190484]

50. Graham DJ, Wagner MS, Castner DG. Information from complexity: Challenges of TOF-SIMS data interpretation. Applied Surface Science. 2006; 252(19):6860–6868.

51. Harvey A, Carr CM, Pereira A. Time-of-flight secondary ion mass spectrometry (ToF-SIMS) analysis of the application of a cationic conditioner to "clean" hair. Journal of cosmetic science. 2004; 55(3):265–79. [PubMed: 15264054]

52. Velardi F, Amante PR, Caniglia M, De Rossi G, Gaglini P, Isacchi G, Palma P, Procaccini E, Zinno F. Osteogenesis induced by autologous bone marrow cells transplant in the pediatric skull. Childs Nerv Syst. 2006; 22(9):1158–66. [PubMed: 16699806]

53. Vavken P, Joshi S, Murray MM. TRITON-X is most effective among three decellularization agents for ACL tissue engineering. Journal of Orthopaedic Research. 2009; 27(12):1612–1618. [PubMed: 19504590]

54. Woods T, Gratzer PF. Effectiveness of three extraction techniques in the development of a decellularized bone-anterior cruciate ligament-bone graft. Biomaterials. 2005; 26(35):7339–49. [PubMed: 16023194]

55. Hudson TW, Liu SY, Schmidt CE. Engineering an improved acellular nerve graft via optimized chemical processing. Tissue Eng. 2004; 10(9–10):1346–58. [PubMed: 15588395]

56. Lewis SA. Everything you wanted to know about the bladder epithelium but were afraid to ask. American journal of physiology. Renal physiology. 2000; 278(6):F867–74. [PubMed: 10836974]

57. Cross WR, Eardley I, Leese HJ, Southgate J. A biomimetic tissue from cultured normal human urothelial cells: analysis of physiological function. American journal of physiology. Renal physiology. 2005; 289(2):F459–68. [PubMed: 15784840]

58. Smith N, Hinley J, Varley C, Eardley I, Trejdosiewicz L, Southgate J. The human urothelial tight junction: claudin 3 and the ZO-1α+ switch. Bladder. 2015; 2(1)

59. Bolland F, Southgate J. Bio-engineering urothelial cells for bladder tissue transplant. Expert Opin Biol Ther. 2008; 8(8):1039–49. [PubMed: 18613757]

60. Scriven SD, Booth C, Thomas DF, Trejdosiewicz LK, Southgate J. Reconstitution of human urothelium from monolayer cultures. The Journal of urology. 1997; 158(3 Pt 2):1147–52. [PubMed: 9258159]

61. Syed O, Walters NJ, Day RM, Kim HW, Knowles JC. Evaluation of decellularization protocols for production of tubular small intestine submucosa scaffolds for use in oesophageal tissue engineering. Acta Biomater. 2014; 10(12):5043–54. [PubMed: 25173840]

62. Wallis JM, Borg ZD, Daly AB, Deng B, Ballif BA, Allen GB, Jaworski DM, Weiss DJ. Comparative assessment of detergent-based protocols for mouse lung de-cellularization and re-cellularization. Tissue Eng Part C Methods. 2012; 18(6):420–32. [PubMed: 22165818]

63. Gilpin SE, Guyette JP, Gonzalez G, Ren X, Asara JM, Mathisen DJ, Vacanti JP, Ott HC. Perfusion decellularization of human and porcine lungs: Bringing the matrix to clinical scale. The Journal of Heart and Lung Transplantation. 2014; 33(3):298–308. [PubMed: 24365767]

64. Wu P, Nakamura N, Kimura T, Nam K, Fujisato T, Funamoto S, Higami T, Kishida A. Decellularized porcine aortic intima-media as a potential cardiovascular biomaterial. Interact Cardiovasc Thorac Surg. 2015; 21(2):189–94. [PubMed: 25972596]

65. Sullivan DC, Mirmalek-Sani SH, Deegan DB, Baptista PM, Aboushwareb T, Atala A, Yoo JJ. Decellularization methods of porcine kidneys for whole organ engineering using a high-throughput system. Biomaterials. 2012; 33(31):7756–64. [PubMed: 22841923]

66. He M, Callanan A, Lagaras K, Steele JA, Stevens MM. Optimization of SDS exposure on preservation of ECM characteristics in whole organ decellularization of rat kidneys. J Biomed Mater Res B Appl Biomater. 2016

67. Ren H, Shi X, Tao L, Xiao J, Han B, Zhang Y, Yuan X, Ding Y. Evaluation of two decellularization methods in the development of a whole-organ decellularized rat liver scaffold. Liver international: official journal of the International Association for the Study of the Liver. 2013; 33(3):448–58. [PubMed: 23301992]

68. Kundu J, Michaelson A, Talbot K, Baranov P, Young MJ, Carrier RL. Decellularized retinal matrix: Natural platforms for human retinal progenitor cell culture. Acta Biomater. 2016; 31:61–70. [PubMed: 26621699]

69. Xu H, Xu B, Yang Q, Li X, Ma X, Xia Q, Zhang Y, Zhang C, Wu Y, Zhang Y. Comparison of decellularization protocols for preparing a decellularized porcine annulus fibrosus scaffold. PLoS One. 2014; 9(1):e86723. [PubMed: 24475172]

70. Santoso EG, Yoshida K, Hirota Y, Aizawa M, Yoshino O, Kishida A, Osuga Y, Saito S, Ushida T, Furukawa KS. Application of detergents or high hydrostatic pressure as decellularization processes in uterine tissues and their subsequent effects on in vivo uterine regeneration in murine models. PLoS One. 2014; 9(7):e103201. [PubMed: 25057942]

71. Mancuso L, Gualerzi A, Boschetti F, Loy F, Cao G. Decellularized ovine arteries as small-diameter vascular grafts. Biomed Mater. 2014; 9(4):045011. [PubMed: 25050540]

72. Gratzer PF, Harrison RD, Woods T. Matrix alteration and not residual sodium dodecyl sulfate cytotoxicity affects the cellular repopulation of a decellularized matrix. Tissue Eng. 2006; 12(10): 2975–83. [PubMed: 17518665]

73. Brown BN, Freund JM, Han L, Rubin JP, Reing JE, Jeffries EM, Wolf MT, Tottey S, Barnes CA, Ratner BD, Badylak SF. Comparison of three methods for the derivation of a biologic scaffold composed of adipose tissue extracellular matrix. Tissue Eng Part C Methods. 2011; 17(4):411–21. [PubMed: 21043998]

74. Rieder E, Kasimir MT, Silberhumer G, Seebacher G, Wolner E, Simon P, Weigel G. Decellularization protocols of porcine heart valves differ importantly in efficiency of cell removal and susceptibility of the matrix to recellularization with human vascular cells. The Journal of thoracic and cardiovascular surgery. 2004; 127(2):399–405. [PubMed: 14762347]

STATEMENT OF SIGNIFICANCE

We report here on the use of a highly sensitive analytical technique, time of flight secondary ion mass spectroscopy (ToF-SIMS) to characterize detergent decellularized scaffolds. ToF-SIMS detected cellular remnants and residual detergent fragments; increased intensity of the detergent fragments correlated with adverse cell matrix interactions. This study demonstrates the importance of maintaining a balance between cell removal and detergent disruption of matrix architecture and matrix surface ligand landscape. This study also demonstrates the power of ToF-SIMS for the characterization of decellularized scaffolds and capability for assessment of decellularization efficacy. Future use of biologic scaffolds in clinical tissue reconstruction will benefit from the fundamental results described in this work.
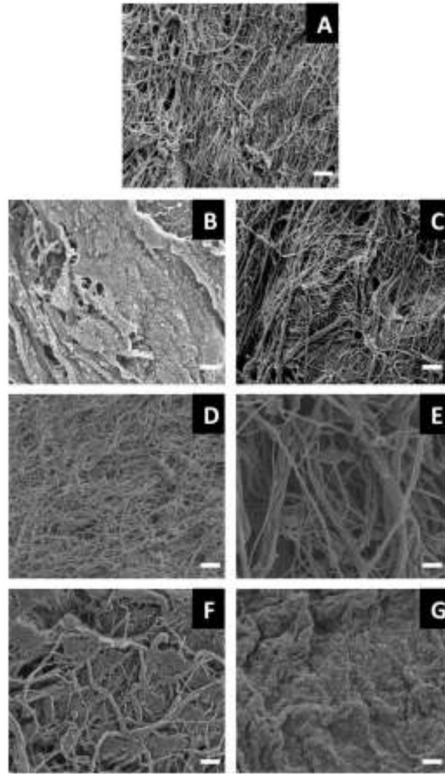
Figure 1.
SEM of the BMC fibre network of UBM samples prepared with (A) water as a no-detergent control, (B) PAA, (C) Triton X-100, (D) CHAPS, (E) sodium deoxycholate, (F) SDS (0.1%) and (G) SDS (1.0%); scale bar represents 1 μm.
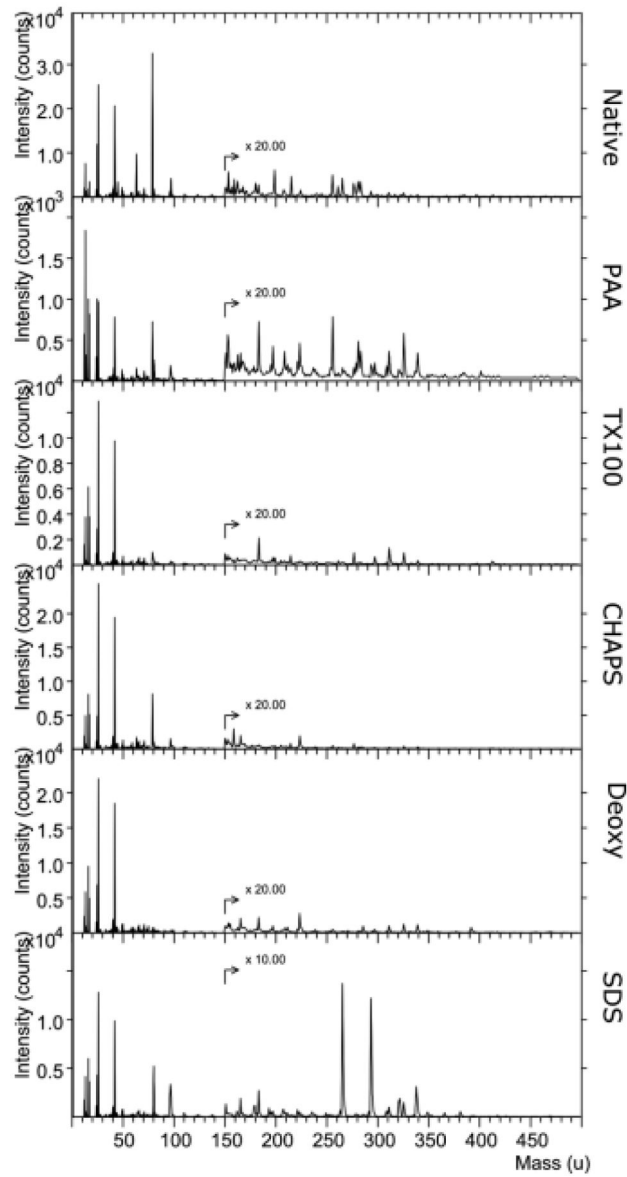
Figure 2.
Representative negative ion spectra of native porcine urinary bladders and bladders treated with PAA, Triton X-100, CHAPS, sodium deoxycholate and SDS (1.0%).
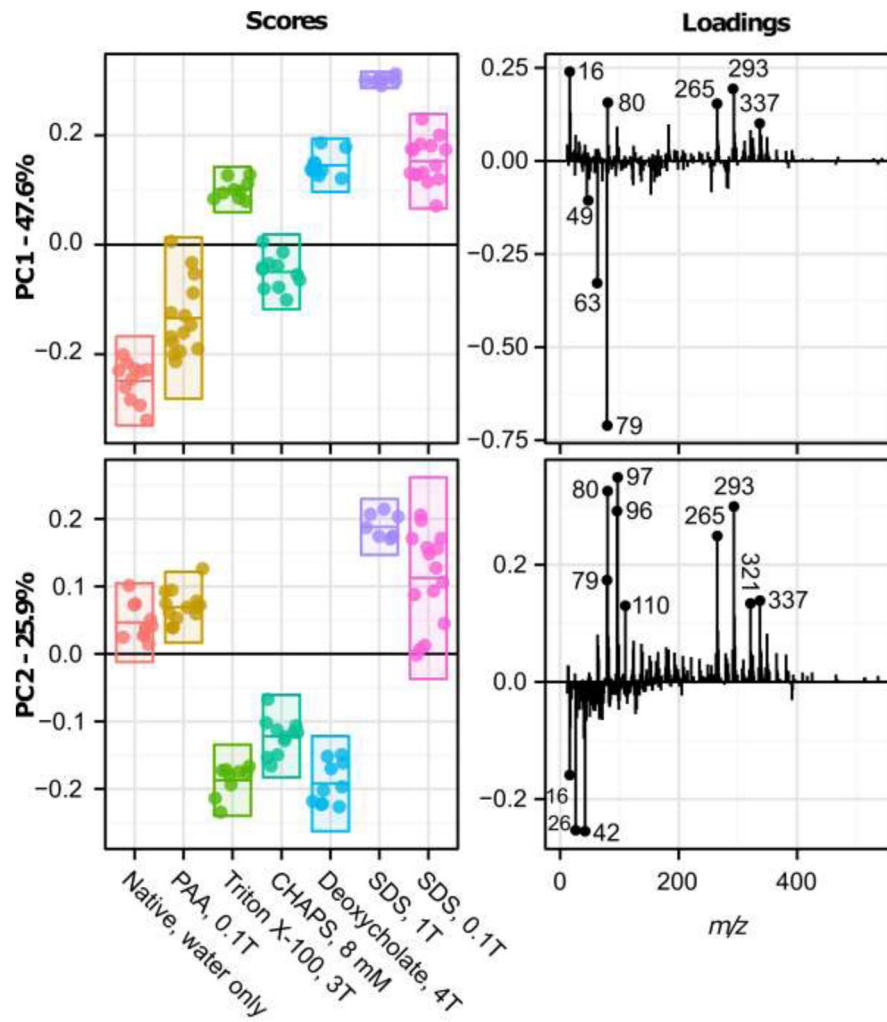
Figure 3.
Principal component analysis (PCA) of negative ion spectra of UBM samples. Scores (left) and loadings (right) plots are shown for the first (top) and second (bottom) principal components which describe 47.6% and 25.9% of variance respectively. In the scores plots, bars represent mean and 95% confidence intervals. In the loadings plots, prominent highly-loading peaks are marked and labelled.
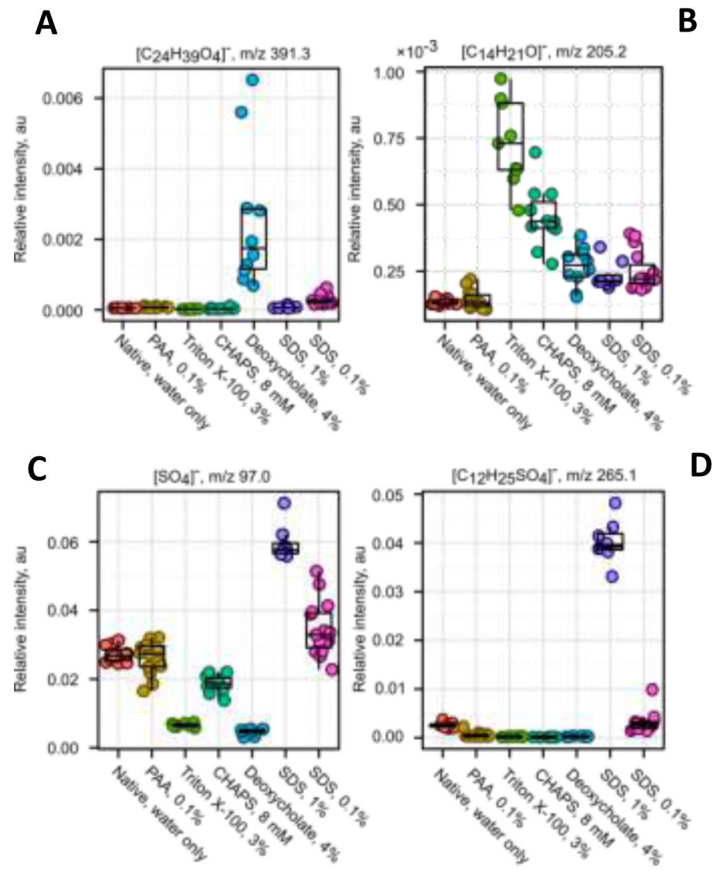
Figure 4.
Peak intensities of residual sodium deoxycholate (A), Triton X-100 (B) and SDS fragments
(C) and (D). All data points are shown. Overlaid box plots show mean (bar), 25th and 75th
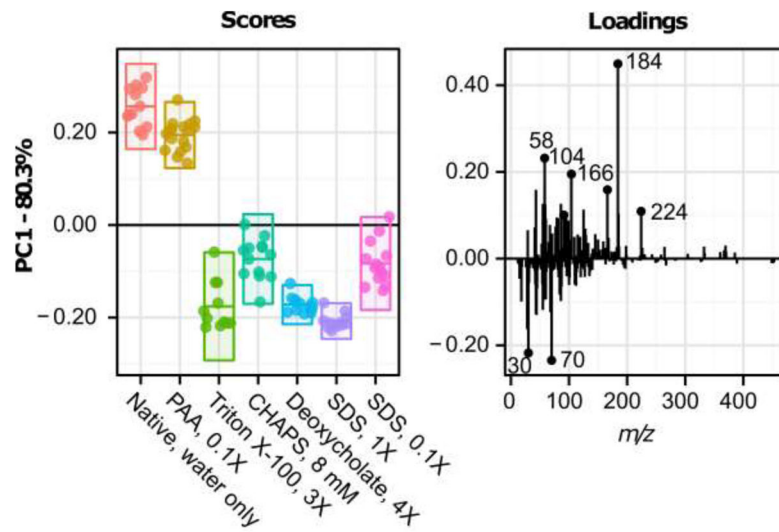quartiles (box) with whiskers extending 1.5 IQR beyond them.

Figure 5.
Principal component analysis (PCA) of positive ion spectra of UBM samples. Scores (left) and loadings (right) plots are shown for the first principal component which described 80.3% of variance. In the scores plot, bars represent mean and 95% confidence intervals. In the loadings plot, prominent highly-loading peaks are marked and labelled.
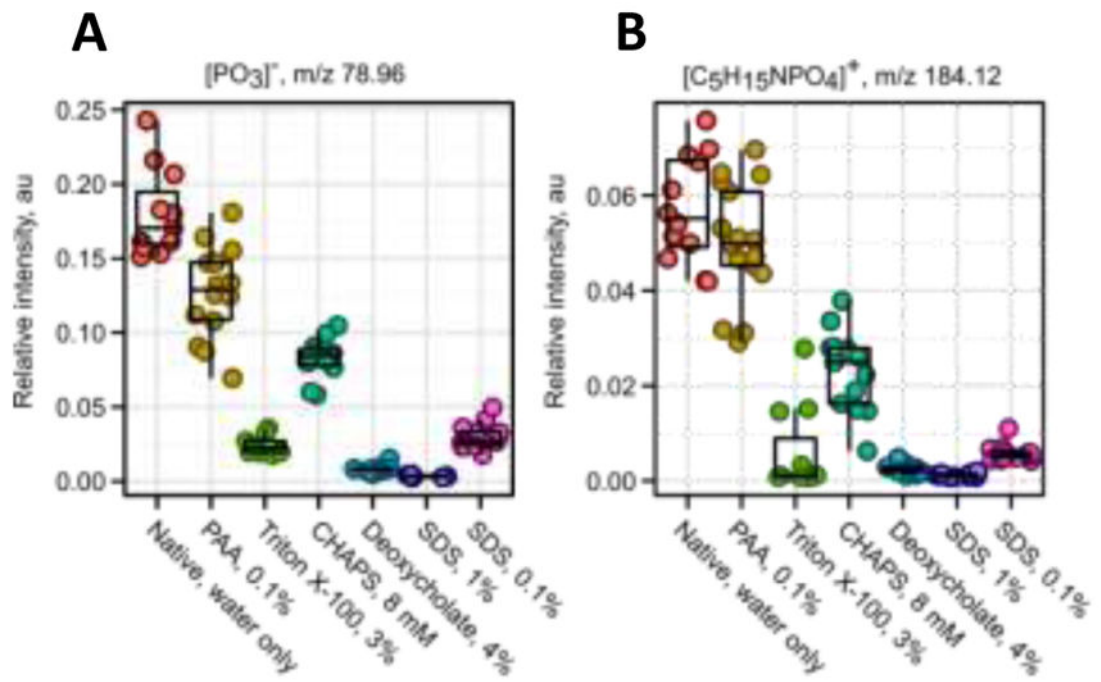
Figure 6.
Peak intensities of cell nuclear (A) and cell membrane (B) associated compounds. All data points are shown. Overlaid box plots show mean (bar), 25th and 75th quartiles (box) with whiskers extending 1.5 IQR beyond them.
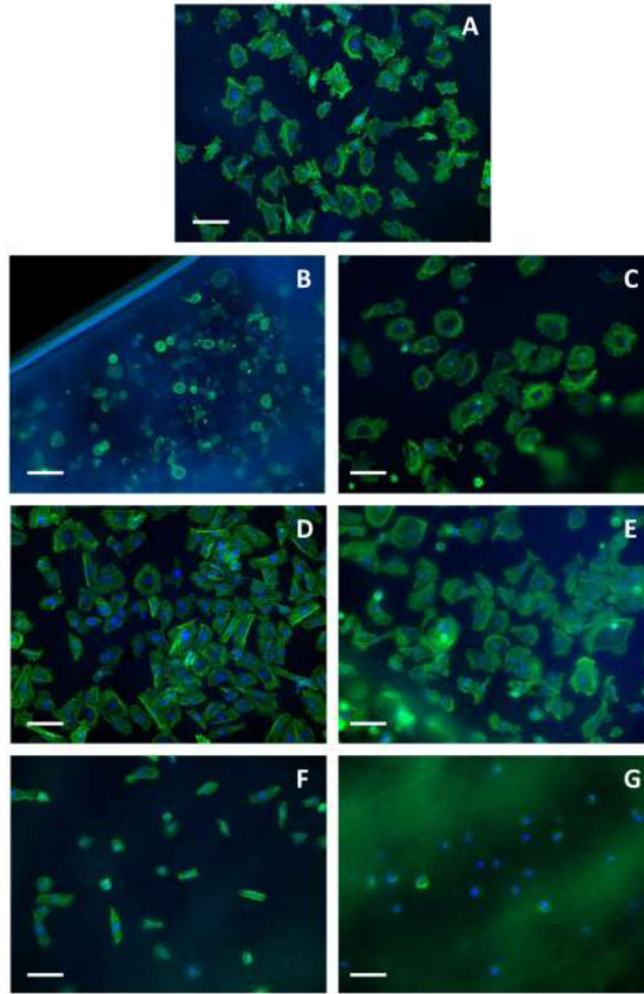
Figure 7.
F-actin cytoskeleton of human urothelial cells cultured on the BMC of porcine urinary bladders prepared with (A) water, (B) PAA, (C) Triton X-100, (D) CHAPS, (E) sodium deoxycholate, (F) SDS (0.1%) and (G) SDS (1.0%); scale bar represents 100 μm.

Table 1

Summary of the polarity, mass, assignment, identity and association of highly loading peaks seen in PCA loadings plots shown in Figures 4 and 6.

Polarity	m/z	Assignment	Identity	Association	PC
Negative	63.0	PO_2^-	Phosphate	Residual nuclear material	1
Negative	79.0	PO_3^-	Phosphate		1
Positive	184.1	$C_5H_{15}NPO_4^+$	Phosphocholine	Residual cell membrane	1
Positive	224.1	$C_9H_{19}NPO_4^+$	Glycerophosphocholine		1
Positive	104.1	$C_5H_{14}NO^+$	Choline		1
Negative	80.0	SO_3^-	Sulphate	SDS headgroup	2
Negative	97.0	SO_4^-			2
Negative	265.1	$C_{12}H_{25}SO_4^-$	Dodecylsulphate	SDS	2
Negative	293.1	$C_{12}H_{25}O_2Na_4^-$	SDS micelle	SDS	2
Negative	391.3	$C_{24}H_{49}O_4$	Deprotonated deoxycholate molecular ion	Deoxycholate	2